Bifurcation of Nonlinear Kelvin Wave–CISK with Conditional Heating in a Truncated Spectral Model: A Possible Mechanism of 30–60–Day Oscillation at the Equator①

Luo Dehai (罗德海)

Department of Atmospheric and Oceanic Sciences, Ocean University of Qingdao, Qingdao 266003

(Received December 12, 1997; revised August 18, 1998)

ABSTRACT

In this paper, the nonlinear Kelvin wave equations with "positive–only" nonlinear (conditional) heating at the equator are reduced to a sixth–order nonlinear ordinary differential equation by using the Galerkin spectral truncated method. The stability analysis indicates that when the heating parameter increases, the supercritical pitchfork and Hopf bifurcations can occur for the prescribed three heating profiles. Numerical calculations are made with the help of the fourth–order Rung–Kutta method. It is found that the convection heating–related Hopf bifurcation can lead to limit cycle and chaotic solutions. In a wide range of heating parameter, the solutions possess 30–60–day periods, and are dominated by wavenumbers one and two, especially by wavenumber–one. In addition, the zonal winds of the low–frequency solutions have a phase reversal between the upper and lower tropospheres. Thus, it appears that the convection heating–related Hopf bifurcation might be a possible mechanism of 30–60–day oscillation in the tropical atmosphere.

Key words: Bifurcation, Wave–CISK, 30–60–day oscillation

1. Introduction

Since the 40–50–day oscillation in the tropical Pacific was first found by Madden and Julian (1971, 1972), it has long been an important research topic. In observational studies, Lau and Chan (1985, 1986), Ghil and Mo (1991) showed that the intraseasonal oscillations in the tropics are dominated by zonal wavenumbers one and two, especially by zonal wavenumber– one. This oscillation is found to propagate slowly eastward along the equator and has maximum amplitude at the equator. Numerous attempts have been made to provide a theoretical explanation for this phenomenon. For example, many investigators attempted to relate the viscous Kelvin wave mode and the Kelvin wave–CISK mode to the tropical (equatorial) intraseasonal oscillation (TIO) (Chang 1977; Lau and Peng 1987; Takahashi 1987; Chang and Lim 1988; Wang 1988; Cho et al. 1994). Although these studies enjoy some success in the explanation of the origin and structures of the TIO, they do not explain all aspects of the TIO. Further, the recent studies done by Lim et al. (1990) and Wang and Xue (1992) showed that the "positive–only" (nonlinear) heating model seems to be able to avoid the scale selection problem. However, a recent analysis by Dunkerton and Crum (1991) and Crum and Dunkerton (1992) seems to suggest that the scale selection problem in the linear Kelvin wave–CISK theory is only modified by the introduction of "positive–only" (nonlinear) heating but not eliminated. Also, they found that when the second–order diffusion is included, the

①The study was supported by the Sichuan Youth Science and Technology Foundation.

scale-dependent damping may be a scale-selection mechanism of the TIO. This indicates that the linear wave-CISK models are not successful in the explanation of the scale-selection of the TIO when the dissipation does not exist or is weaker. Thus, it is necessary to develope a nonlinear wave-CISK model, which helps us to understand the dynamical mechanism of the TIO. In a highly truncated spectral model of the nonlinear shallow-water system of equations on the equatorial β-plane, Van Tuyl (1987) studied nonlinearities in the low-frequency equatorial waves, and found that for the prescribed forcing the horizontal advection, at least within the context of the shallow-water model, does not substantially affect either the standing wave or the propagating components of the 40-day oscillation. Especially, he noted that the inclusion of the interactive latent release would give rise to rather complex nonlinear behaviour not observed in his study. Zhao and Ghil (1991) studied nonlinear symmetric instability (NSI) in the equatorial region by considering the advective nonlinearity, and tried to apply the NSI to explain the 24-28-day oscillation along the equator. But this NSI model is not capable of explaining the "wavenumber-1 or -2" structure of 40-50-day oscillation mostly found in the Indian Ocean and the western Pacific. More recently, with the help of the Galerkin truncated spectral representation Luo (1996) investigated the finite-amplitude Kelvin wave-CISK modes with the traditional wave-CISK heating and tried to explain the preference scale-selection of intraseasonal oscillation. However, unfortunately, he did not discuss how the 30-60-day oscillation occurs.

In this paper, we will investigate the bifurcation problem of the nonlinear Kelvin wave-CISK with the "positive-only" nonlinear heating, and try to apply the obtained Hopf bifurcation to explain the occurrence of 30-60-day low frequency oscillation at the equator. The main outline is as follows. In Section 2, the nonlinear motion equations describing the nonlinear Kelvin wave-CISK modes with the " positive-only" nonlinear (conditional wave-CISK) heating are introduced. In Section 3, the three vertical profiles of the convection heating are prescribed, and a sixth-order nonlinear ordinary differential equation is obtained by using the Galerkin spectral truncated method. The Hopf bifurcations and stability analyses for the symmetric and asymmetric heating profiles are made in Sections 4 and 5 respectively, and their numerical results are also given in the two sections. In Section 6, we give the vertical structure of the nonlinear Kelvin wave-CISK mode with wavenumber-one for the symmetric heating profile. Conclusion and discussions are given in Section 7.

2. Nonlinear equations of the Kelvin waves at the equator, conditional wave-CISK heating and truncated spectral equations

2.1 *Nonlinear equations of the Kelvin waves at the equator and conditional wave-CISK heating*

A lot of observations had indicated that the TIO has its maximum amplitude at the equator (Van Tuyl 1987; Hayashi and Golder 1993). Lim et al. (1990), Wang and Xue (1992), Dunkerton and Crum (1991) showed that the linear two-level CISK with conditional heating yields nonpropagating unstable waves and propagating stable waves depending on the magnitude of the heating forcing. But in the three-level model, instability and zonal propagation occur due to the coalescence of vertical modes (Chang and Lim, 1988). In particular, Dunkerton and Crum (1991) found that the nonlinear dynamical effects may be important for the zonal propagation of the TIO. Further, Van Tuyl (1987) found that the nonlinear influences tend to be more confined near the equator. Based on these discussions, the baroclinic nonlinear Kelvin wave model with conditional heating at the equator is applied in this paper.

In the equatorial region, the nonlinear equations of the Kelvin waves with the conditional wave-CISK heating, friction and the Newtonian cooling can be written in the form

$$\left(\frac{\partial}{\partial t}+u\frac{\partial}{\partial x}+w\frac{\partial}{\partial z}\right)\frac{\partial u}{\partial z}=-\frac{\partial\theta}{\partial x}-\mu\frac{\partial u}{\partial z}\ , \tag{1a}$$

$$\frac{\partial u}{\partial x}+\frac{\partial w}{\partial z}=0\ , \tag{1b}$$

$$\left(\frac{\partial}{\partial t}+u\frac{\partial}{\partial x}+w\frac{\partial}{\partial z}\right)\theta+N^2w=N^2\eta(z)\frac{1}{2}(w+|w|)|_{z=z_0}-\gamma\theta\ , \tag{1c}$$

where u and w are the disturbance volecities in the zonal and vertical directions respectively, N is the *Brunt-Vaisala* frequency, $\eta(z)$ is the vertical profile of convective heating, $\theta=g\frac{\theta'}{\theta_0}=\frac{\partial\varphi}{\partial z}$ is the hydrostatic balance relation of the large-scale motion, θ' is the disturbance potential temperature, g is the acceleration speed due to gravity, θ_0 is the mean potential temperature, φ is the gravity potential, z_0 is the height of convective heating, μ and γ are the friction and Newton coefficients respectively. Similar to Zhao and Ghil (1991), we may assume $\mu=\gamma$. In equations (1a-1c), a wave-CISK scheme with conditional (positive-only) heating was applied. For this scheme, heating only occurs in the region of the upward motion, which has been used by Lim et al. (1990) and Crum and Dunkerton (1992). If $\mu=\gamma=0$ and $\frac{1}{2}(w+|w|)|_{z=z_0}$ is replaced by $W|_{z=z_0}$, Equations (1a-1c) reduce to those used by Luo (1996). When the nonlinear advection terms are not considered, they reduce to the linear Kelvin wave-CISK model derived by Takahashi (1987) if $\frac{1}{2}(w+|w|)|_{z=z_0}$ in Eq.(1c) is replaced by $W|_{z=z_0}$.

According to Eq.(1b), we introduce ψ so that it satisfies $u=-\frac{\partial\psi}{\partial z}$ and $w=\frac{\partial\psi}{\partial x}$. In this case, Eqs.(1a-1c) can be rewriten as

$$\frac{\partial}{\partial t}\frac{\partial^2\psi}{\partial z^2}+J(\psi,\frac{\partial^2\psi}{\partial z^2})=\frac{\partial\theta}{\partial x}-\mu\frac{\partial^2\psi}{\partial z^2}\ , \tag{2a}$$

$$\frac{\partial\theta}{\partial t}+J(\psi,\theta)+N^2\frac{\partial\psi}{\partial x}=N^2\eta(z)\frac{1}{2}(\frac{\partial\psi}{\partial x}+\left|\frac{\partial\psi}{\partial x}\right|)|_{z=z_0}-\mu\theta\ , \tag{2b}$$

where $J(a,b)=\frac{\partial a}{\partial x}\frac{\partial b}{\partial z}-\frac{\partial a}{\partial z}\frac{\partial b}{\partial x}$ is the Jacobian operator, ψ and θ vanish at $z=0$ and H.

Introduce the nondimensional quantities as follows:

$$(x,z)=(Lx^*,Hz^*),\ \psi=HU\psi^*,\ \theta=\bar{\theta}\theta^*,\ t=\frac{L}{U}t^*\ , \tag{3}$$

where the asterisks denote nondimensional form, U and L are the horizontal characteristic velocity and length scales respectively, H is the vertical characteristic length scale, $\bar{\theta}=g\frac{\bar{\theta}_d}{\theta_0}$, $\bar{\theta}_d$ is the characteristic quantity of the disturbance potential temperture.

The nondimensionalization is made by substituting (3) to Eqs.(2a–2c), and the dropping of "*" leads to

$$\frac{\partial}{\partial t}\frac{\partial^2\psi}{\partial z^2} + J(\psi, \frac{\partial^2\psi}{\partial z^2}) = C_A\frac{\partial\theta}{\partial x} - R_a\frac{\partial^2\psi}{\partial z^2} \ , \tag{4a}$$

$$\frac{\partial\theta}{\partial t} + J(\psi, \theta) + C_d\frac{\partial\psi}{\partial x} = C_d\eta(z)\frac{1}{2}(\frac{\partial\psi}{\partial x} + \left|\frac{\partial\psi}{\partial x}\right|)|_{z=z_0} - R_a\theta \ , \tag{4b}$$

where $C_A = \frac{H\bar{\theta}}{U^2}$, $C_d = \frac{N^2H}{\bar{\theta}}$, $R_a = \mu\frac{L}{U}$, z_0 is the nondimensional height of convective heating. The variables in Eqs.(4a–4b) vanish at $z = 0$ and 1.

When the nonlinear and dissipation terms are excluded in Eqs.(4a–4b), and when the convective heating is not strong and increases, the phase speed of the Kelvin wave–CISK mode is decreased so as to keep its slow eastward zonal propagation. However, when the convective heating is strong, the nonpropagating unstable modes occur. Interestingly, in nonlinear framework nonlinear interaction can lead to the finite–amplitude oscillation even when the convective heating is very strong (Zhao and Ghil, 1991). By using the multiple–scale method Zhao and Ghil (1991) studied the finite–amplitude oscillation in the neighbourhood of a critical value where a critical value occurs for stationary instability. Clearly, when their parameter is far above the critical value, the multiple–scale method cannot be applied to investigating the finite–amplitude oscillation. However, the truncated spectral method is applicable for this case (Yost and Shirer, 1982). In Eqs.(4a–4b), when $\frac{\partial^2\psi}{\partial z^2}$ and $\eta(z)(\frac{\partial\psi}{\partial x} + \left|\frac{\partial\psi}{\partial x}\right|)|_{z=z_0}$ are replaced by the terms $\frac{\partial^2\psi}{\partial x^2} + \frac{\partial^2\psi}{\partial z^2}$ and $b\frac{\partial\psi}{\partial x}$ respectively, these equations are identical in form to the nonlinear equations describing the Be'nard cell flow problem studied by Lorenz (1963). Because the TIO has its maximum amplitude at the equator, the circulation flow of the TIO along the latitude circle at the equator can be considered as a Be'nard cell flow. In this case, the truncated spectral method proposed by Lorenz (1963) can be applied to investigate the dynamical mechanism of the TIO. Obviously, this method here fails to study the horizontal structure and the meridional propagation of the TIO. In a shallow–water model, a similar truncated spectral method had been successfully applied to investigating the horizontal structures and the zonal propagation of the TIO (Van Tuyl, 1987).

3. The vertical profile of convective heating and the spectral equations

3.1 *The vertical profile of convective heating and the choice of spectral functions*

Takahashi (1987) had shown that the vertical distribution of the non–dimensional heating parameter $\eta(z)$ in the wave–CISK is very important to the slow phase speed of the TIO. This point had been confirmed by Lau and Peng (1987), Chang and Lim (1988), Lim et al. (1990) and Crum and Dunkerton (1992).

Similar to Crum and Dunkerton (1992), the vertical profile of the convective heating $\eta(z)$ is defined by

$$\eta(z) = \eta_0 e^{-\delta z}\sin(\pi z) \ , \tag{5}$$

where η_0 denotes the intensity of convective heating (also called "heating parameter") that measures the availability of water vapor for convergence and the efficiency of release of the latent heat by cumulus convection (Dunkerton and Grum, 1991; Zhao and Weare 1994). Note that this vertical profile is a half-sine wave adjusted by the parameter δ to vary the level of maximum heating. When $\delta > 0$, the maximum heating is located in the lower layer of the troposphere, which is also called "shallow convective heating", while when $\delta < 0$, the maximum heating is located in the upper layer of the troposphere and is also called "deep convective heating". The two convective heatings are totally named by "asymmetric convective heating". However, when $\delta = 0$, the maximum of this heating profile is in the midtroposphere, which is also called "symmetric convective heating".

Because the value of η_0 does not affect the vertical distribution of the convective heating, the parameter η_0 can be prescribed so that the vertical distribution of the heat profile $\eta(z)$ can be obtained. As an example, if we choose $\delta = 2, 0$ and -2, for $\eta_0 = 1.0$ the vertical profile of the convective heating $\eta(z)$ is shown in Fig. 1.

It is found from Fig. 1 that for $\delta = 2$, the maximum heating center of the convective heating is found to be in the lower layer of the troposphere. When $\delta = -2.0$, the maximum heating is located in the upper layer of the troposphere, which is consistent with the vertical profile of the convective heating prescribed by Lau and Peng (1987). When $\delta = 0$, the maximum heating is located in the middle layer of the troposphere, which is almost the same as the sine-wave profile of the vertical convective heating used by Takahashi (1987). In this paper, for the prescribed three heating profiles we will investigate the dynamical behaviour of the nonlinear Kelvin wave–CISK at the equator. It is found from the comparison with the heating profiles used in Luo (1996) that the three heating profiles given here are slightly different from their heating profiles. On the other hand, it should be pointed out that in the 3-layer linear wave–CISK model studied by Takahashi (1987), the heat parameter η_2 (the value of the heat parameter $\eta(z)$ at the upper level of the troposphere) is allowed to vary between 0 and 10. In this paper, the parameter $\frac{\eta_0}{2} e^{-\delta}$ is identical to his parameter η_2. Here, in order to see clearly the bifurcation properties of the nonlinear Kelvin wave–CISK, the heat parameter η_0 is chosen to vary arbitrarily. Of course, this assumption cannot be completely accepted and has an inconsistency with the observational facts of the TIO.

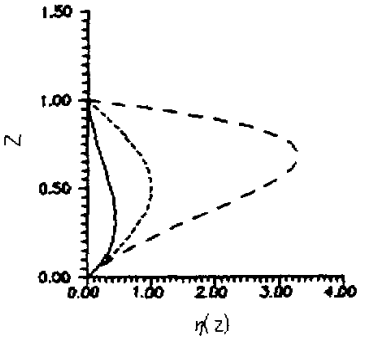

Fig. 1. The vertical distribution of convective heating: The solid curve corresponds to $\delta = 2$; the short dashed curve denotes $\delta = 0$; the long dashed curve corresponds to $\delta = -2.0$.

Because both Kelvin wave–CISK modes and vertical convective heating have apparent baroclinic structure, for simplicity we consider two baroclinic modes in the vertical direction (Chang and Lim, 1988). Here, we will apply the truncated spectral method proposed by Lorenz (1963) and used by many investigators to simplify Eqs.(4a–4b). According to Lorenz (1963), the spectral truncated solutions to Eqs.(4a–4b) may be assumed to be

$$\psi = -x_1(t)\sin(kx)\sin(\pi z) - x_2(t)\sin(kx)\sin(2\pi z) \ , \tag{6a}$$

$$\theta = x_3(t)\cos(kx)\sin(\pi z) + x_4(t)\cos(kx)\sin(2\pi z) - x_5(t)\sin(2\pi z) - x_6(t)\sin(4\pi z) \ , \tag{6b}$$

where $k = \dfrac{n_0}{6.371}$ is the zonal wavenumber of the Kelvin wave–CISK mode. If we choose $n_0 = 1$, k denotes zonal wavenumber–one. While $n_0 = 2$, it denotes zonal wavenumber–two. In (6a–6b), $x_1(t)$ and $x_3(t)$ represent the first baroclinic modes of the streamfunction and potential temperture fields respectively, $x_2(t)$, $x_4(t)$ and x_5 denote the second baroclinic modes, while $x_6(t)$ denotes the third baroclinic mode. Note that, the second baroclinic mode $x_4(t)$ is induced by the interaction between two first baroclinic modes $x_1(t)$ and $x_3(t)$, while the third baroclinic mode $x_6(t)$ is induced by the interaction between two second baroclinic modes $x_2(t)$ and $x_4(t)$. When $x_2(t) = x_4(t) = x_6(t) = 0$, Eqs.(6a–6b) reduce to the spectral truncated solutions proposed by Lorenz (1963), who studied the nonperiodic Be'nard convection flow. Takahashi (1987) pointed out that the first baroclinic mode $x_1(t)$ can describe the reverse phase structure of the intraseasonal oscillation between the upper and lower layers. However, when a convective heating exists in the upper or lower layer of the troposphere, the higher–order baroclinic modes can be induced by the interaction between the lower baroclinic modes. Therefore, in order to investigate the nonlinear dynamical behaviour of the Kelvin wave–CISK–Kelvin mode, we should consider the role of $x_2(t)$, $x_4(t)$ and $x_6(t)$. In this case, Eqs.(6a–6b) are the generalization of the Lorenz's (1963) spectral truncated solutions. It should be pointed out that the spectral truncated solutions Eqs.(6a–6b) are actually the approximate solutions of the nonlinear equations (4a–4b), which contain the terms of the nonlinear interaction among the finite–amplitude modes.

3.2 *The six–coefficient spectral equations for asymmetric and symmetric heating profiles*

Substituting (6a–6b) into Eqs.(3a–3b), we can obtain the six–coefficient spectral equations in the form

$$\frac{dx_1}{dt} = -\frac{C_A k}{\pi^2} x_3 - R_a x_1 \ , \tag{7a}$$

$$\frac{dx_2}{dt} = -\frac{C_A k}{4\pi^2} x_4 - R_a x_2 \ , \tag{7b}$$

$$\frac{dx_3}{dt} = \pi k x_1 x_5 + C_d k \lambda_1 x_1 - C_d k \lambda_2 x_2 - R_a x_3 \ , \tag{7c}$$

$$\frac{dx_4}{dt} = 2\pi k x_2 x_6 + k C_d \delta_1 x_2 - k C_d \delta_2 x_1 - R_a x_4 \ , \tag{7d}$$

$$\frac{dx_5}{dt} = -\frac{k\pi}{2}x_1x_3 - R_a x_5 \ , \tag{7e}$$

where

$$\lambda_1 = 1 - \frac{\eta_0}{2}\frac{(1-e^{-\delta})}{\delta}\left[1 - \frac{1}{1+\left(\frac{2\pi}{\delta}\right)^2}\right]\sin(\pi z_0) \ ,$$

$$\lambda_2 = \frac{\eta_0}{2}\frac{(1-e^{-\delta})}{\delta}\left[1 - \frac{1}{1+\left(\frac{2\pi}{\delta}\right)^2}\right]\sin(2\pi z_0) \ ,$$

$$\delta_1 = 1 - \frac{\eta_0}{2}\frac{(1+e^{-\delta})}{\delta}\left[\frac{1}{1+\left(\frac{\pi}{\delta}\right)^2} - \frac{1}{1+\left(\frac{3\pi}{\delta}\right)^2}\right]\sin(2\pi z_0) \ ,$$

$$\delta_2 = \frac{\eta_0}{2}\frac{(1+e^{-\delta})}{\delta}\left[\frac{1}{1+\left(\frac{\pi}{\delta}\right)^2} - \frac{1}{1+\left(\frac{3\pi}{\delta}\right)^2}\right]\sin(\pi z_0) \ .$$

When $\delta = 0$ (symmetric heating), $\lambda_1 = \beta_1 = 1 - \frac{\eta_0}{2}\sin(\pi z_0)\lambda_2 = \beta_2 = \frac{\eta_0}{2}\sin(2\pi z_0)\delta_1 = 1$ and $\delta_2 = 0$. It is found from Eqs.(7a–7f) that for a symmetric heating profile, the equations of the variables $x_2(t)$, $x_4(t)$ and $x_6(t)$ do not depend on the variables $x_1(t)$, $x_3(t)$ and $x_5(t)$. In this case, if we choose $x_2(t) = x_4 = x_6 = 0$, Eqs.(7a–7f) reduce to the Lorenz's (1963) equations.

When $\delta \neq 0$, Eqs.(7a–7f) describe nonlinear interaction between the vertical Kelvin wave–CISK modes for the asymmetric heating profile. Obviously, the equations of the variables $x_2(t)$, $x_4(t)$ and $x_6(t)$ can be related to the variables $x_1(t)$, $x_3(t)$ and $x_5(t)$ through the parameters λ_2 and δ_2. Here, if the chosen atmospheric parameters are $L = 10^3$ km, $U = 10$ m / s, $H = 10$ km, $\bar{\theta}_d = \frac{\bar{\theta}}{g}$, $N = 10^{-2}$ s^{-1}, $n_0 = 1$ or 2 and $z_0 = 0.103$ (Miyahara, 1987), then $C_A = 100$ and $C_A = 1.0$. While η_0 is considered as a controlling parameter. On the other hand, in this paper we consider the case of weaker dissipation so that the periodic solutions of system (7) without nonlinearity can be found in the case without the convective heating. For example, $R_a = 0.0001$ is chosen in this paper.

4. Dynamic behaviour of nonlinear Kelvin wave–CISK for symmetric heating profile

4.1 *The Hopf bifurcation and stability analysis for symmetric heating profile*

With $P = (\bar{x}_1, \bar{x}_2, \bar{x}_3, \bar{x}_4, \bar{x}_5, \bar{x}_6)$, when $\beta_1 > 0$, system (7) has one stationary solution $P_0 = (0, 0, 0, 0, 0, 0)$. When $\beta_1 < 0 (\gamma = 2(\frac{C_A C_d}{\pi^4}\beta_1 + \frac{R_a^2}{\pi^2 k^2}) \approx 2\frac{C_A C_d}{\pi^4}\beta_1 < 0)$, system (7) has three stationary solutions:

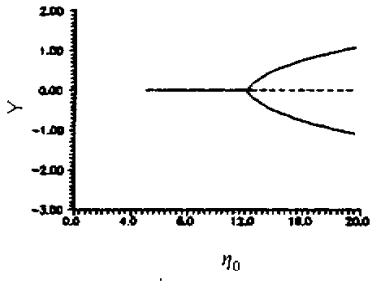

Fig. 2. Bifurcation diagram of stationary solution $Y = \bar{x}_1$ for zonal wavenumber-one with the heating parameter η_0. Stable solution branches are solid, unstable one is dashed.

$$P_0 = (0,0,0,0,0,0),\ P_{1,2} = \left(\pm\sqrt{-\gamma}, 0, \mp\frac{R_a\pi^2}{C_A k}\sqrt{-\gamma}, 0, \pm\frac{\pi^3}{2C_A}\sqrt{-\gamma}, 0\right). \tag{8}$$

If one defines $\bar{x}_1 = Y$, then the bifurcation tree of the variable $\bar{x}_1$ with the heating parameter η_0 is shown in Fig. 2.

It is found that when the heating parameter η_0 is small, and $\beta_1 > 0$, system (8) has only one stationary solution P_0. However, when η_0 increases and $\beta_1 < 0$, the stationary solution is bifurcated into three stationary solutions P_0 and $P_{1,2}$.

From the nonlinear equations (7a–7f) we obtain the stability matrix of the spectral equations for the symmetric heating in the form

$$M = \begin{bmatrix} -R_0 & 0 & -\frac{C_A k}{\pi^2} & 0 & 0 & 0 \\ 0 & -R_0 & 0 & -\frac{C_A k}{4\pi^2} & 0 & 0 \\ C_d k\beta_1 + \pi k\bar{x}_5 & -C_d k\beta_2 & -R_0 & 0 & \pi k\bar{x}_1 & 0 \\ 0 & C_d k & 0 & -R_0 & 0 & 0 \\ -\frac{k\pi\bar{x}_3}{2} & 0 & -\frac{k\pi\bar{x}_1}{2} & 0 & -R_0 & 0 \\ 0 & 0 & 0 & 0 & 0 & -R_0 \end{bmatrix} \tag{9}$$

in this case we further obtain

$$(\omega + R_a)^3\{(\omega + R_a)^3 + \frac{C_A k}{\pi^2}[\frac{\pi^4 k}{C_A}\bar{x}_1^2 + C_d k\beta_1](\omega + R_a) + \frac{\pi^2 k^2}{2}R_a\bar{x}_1^2\} = 0\ . \tag{10}$$

For $\beta_1 > 0$, system (7) has one stationary solution P_0. It is clearly found from (10) that for $\beta_1 > 0$, the stationary solution P_0 is stable. For $\beta_1 < 0$, system (7) has three stationary solutions P_0 and $P_{1,2}$. It is shown that the stationary solution P_0 is unstable, while the stationary solutions $P_{1,2}$ are stable. Here, because $R_a \to 0$, according to Jin and Ghil (1990), the three roots of Eq.(10) can be expressed by

$$\omega_{1,2} = \pm i\sqrt{\Delta} - \frac{R_a}{2} \ , \tag{11a}$$

$$\omega_3 = -\frac{3R_a}{2} \ , \tag{11b}$$

where $\Delta = -\frac{C_A C_d k^2}{\pi^2}\beta_1$.

In (11a), it is found that when the heating parameter η_0 is larger, and $\beta_1 < 0$, then $\Delta > 0$. In this case, $\mathrm{Re}(\omega_{1,2}) = -\frac{R_a}{2} < 0$ and $\mathrm{Im}(\omega_{1,2}) \neq 0$. According to the bifurcation theory (Marsden and McCracken, 1976; Guckenheimer and Holmes, 1983), when the parameter β_1 changes from $\beta_1 > 0$ to $\beta_1 < 0$, a supercritical pitchfork bifurcation will occur, that is, when η_0 gradually increases so that the parameter β_1 changes its sign, a supercritical pitchfork bifurcation occurs at $\beta_1 = 0$ (Zhao and Ghil, 1991), which is shown in Fig. 2. To show this point, we will give its numerical result in the following subsection.

4.2 *Numerical results*

In Eqs.(7a–7f), without the loss of generality, we choose the initial data $x_1(0) = 0.6$, $x_2(0) = 0.3$ and $x_3(0) = x_4(0) = x_5(0) = x_6(0) = 0.0$. For the symmetric heating profile ($\delta = 0$), a fourth-order Rung-Kutta method is used to solve numerically Eqs.(7a–7f). As pointed out by Takahashi (1987), because the first baroclinic mode $x_1(t)$ can describe the reverse phase structure of the zonal winds between the upper and lower layers in an intraseasonal oscillation, the time evolution of $x_1(t)$ and the phase trajectory in the (x_1, x_3) -plane for the solutions of system (7) are only given. If we choose $n_0 = 1$, then for zonal wavenumber-one the evolutions of $x_1(t)$ and the phase trajectories in the (x_1, x_3)-plane for the solutions of system (7) for $\eta_0 = 0$, 0.4, 4.0, 9.0, 21.0 and 33.0 are shown in Figs. 3 and 4, respectively.

It is clearly found from Figs. 3 and 4 that for $\eta_0 = 0.0$, the projection onto (x_1, x_3)-plane of trajectory of the system (7) is found to be a periodic limit cycle with 15-day period. When η_0 increases, repeated bifurcation with period doubling occurs. For example, when $\eta_0 = 0.4$, a double-period limit cycle is found, and has two principal periods corresponding to 15 and 30 days, respectively. While $\eta_0 = 4.0$, the phase trajectory in the (x_1, x_3)-plane becomes a quadruple-period limit cycle, and the period of $x_1(t)$ is found to be within the range from 20 to 35 days. However, when $\eta_0 = 9.0$, the principal period of $x_1(t)$ is near 30 days. Afterwards, when η_0 further becomes larger, the chaotic solutions can be detected. For example, for $\eta_0 = 21.0$, the solution $x_1(t)$ exhibits chaotic behaviour, and its phase trajectory in the (x_1, x_3)-plane is found to be stranger attractor. For this case, the oscillation period of $x_1(t)$ is about 30–50-days, which belongs to the intraseasonal band. When $\eta_0 = 33.0$, the chaotic solution of $x_1(t)$ is more clear, and its period is in the 30–60-day band. Thus, it is clear from these figures that, as the heating prameter η_0 increases, a period-doubling cascade leads to the chaotic solutions (Feigenbaum, 1978; Lin et al., 1989; Jin and Ghil, 1990). In a wide parameter domain, the chaotic solutions possess 30–60-day period. For zonal wavenumber-two, a 30-day oscillation can be observed in a narrower parameter domain (figures omitted). However, for zonal wavenumber-three, no 30–60-day oscillation can be detected. Therefore, in our nonlinear model, 30–60-day disturbances are mainly limited to the "wavenumber-1" structure. In the linear CISK model proposed by Chang and Lim

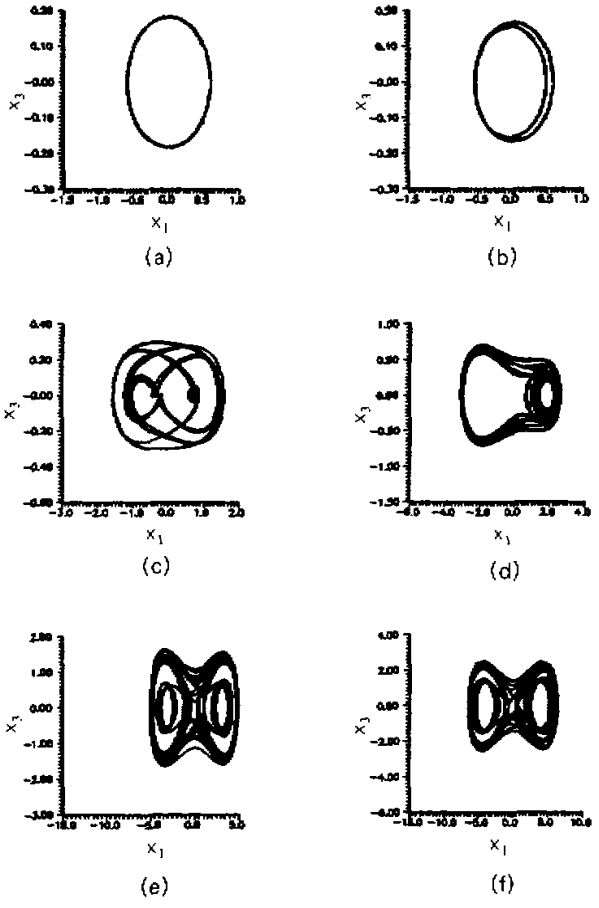

Fig. 3. The phase trajectories in the (x_1, x_3)-plane for the solutions of system (7) for (a) $\eta_0 = 0.0$, (b) $\eta_0 = 0.4$, (c) $\eta_0 = 4.0$, (d) $\eta_0 = 9.0$, (e) $\eta_0 = 21.0$ and (f) $\eta_0 = 33.0$.

(1988), their result can satisfactorily explain the general characteristics of the simulated low-frequency disturbances, but cannot explain the persistence of the "wavenumber-1" structure of the simulated 30-60-day disturbances. Here, our numerical results indicate that when the maximum heating is located in the middle layer of the troposphere, the "wavenumber-1" 30-60-day low-frequency oscillation at the equator can be excited through the convection heating-related Hopf bifurcation.

5. Dynamic behaviour of nonlinear Kelvin wave-CISK for asymmetric heating profile

5.1 *The Hopf bifurcation and stability analysis*

If we set $\frac{dx_i}{dt} = 0 (i = 1, 2, \cdots, 6)$, the stationary solutions of system (7) are obtained as

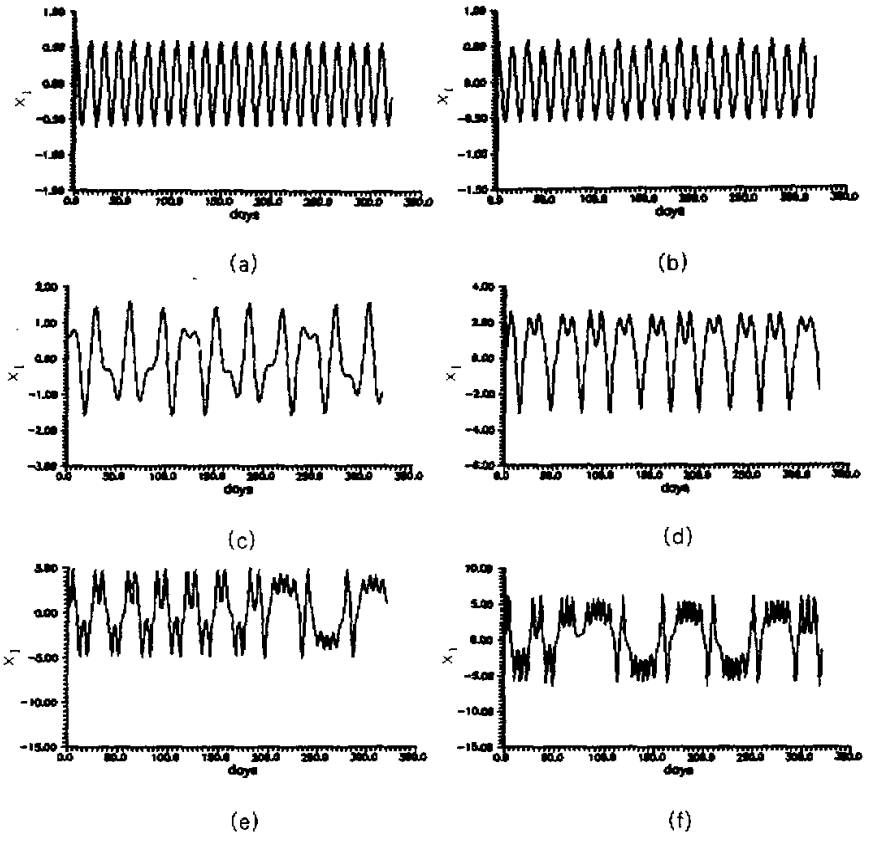

Fig. 4. The time evolution of $x_1(t)$ corresponding to Figs. 3a–3f: (a) $\eta_0 = 0.0$, (b) $\eta_0 = 0.4$, (c) $\eta_0 = 4.0$, (d) $\eta_0 = 9.0$, (e) $\eta_0 = 21.0$ and (f) $\eta_0 = 33.0$.

$$P_0 = (0, 0, 0, 0, 0, 0),\ P_{1,2} = \left(\bar{x}_1, \bar{x}_2, -\frac{\pi^2 R_a}{C_A k}\bar{x}_1, -\frac{4\pi^2 R_a}{C_A k}\bar{x}_2, \frac{\pi^3}{C_A}\bar{x}_1^2, \frac{4\pi^3}{C_A}\bar{x}_2^2\right), \tag{12}$$

and $\bar{x}_1$ and $\bar{x}_2$ satisfy the following two equilibrium solution equations:

$$\left(\frac{\pi^4 k}{2C_A}\bar{x}_1^2 + C_d k\lambda_1 + \frac{\pi^2 R_a^2}{C_A k}\right)\bar{x}_1 = C_d k\lambda_2 \bar{x}_2\ , \tag{13a}$$

$$\left(\frac{8\pi^4 k}{C_A}\bar{x}_2^2 + C_d k\delta_1 + \frac{4\pi^2 R_a^2}{C_A k}\right)\bar{x}_2 = C_d k\delta_2 \bar{x}_1\ . \tag{13b}$$

By eliminating the variable $\bar{x}_2$ in Eqs.(13a–13b), a nonlinear algebraic equation for $\bar{x}_1$ can be obtained. For this algebraic equation, its solution can be obtained by a numerical scheme.

Similar to Section 4,we can obtain the eigenvalue equation of system (7) in the form

$$(\omega + R_a)^6 + a_1(\omega + R_a)^4 + a_2 R_a(\omega + R_a)^3 + a_3(\omega + R_a)^2 + a_4 R_a(\omega + R_a) + R_a^2 a_5 = 0 \ , \tag{14}$$

where

$$a_1 = \frac{C_A k}{4\pi^2}(4P + Q) \ , \quad a_2 = \frac{\pi^2 k^2}{2}(\bar{x}_1^2 + 4\bar{x}_2^2) \ , \quad a_3 = \frac{C_A^2 k^2}{4\pi^4}(PQ - C_d^2 k^2 \lambda_2 \delta_2) \ ,$$

$$a_4 = \frac{C_A k^3}{8}(Q\bar{x}_1^2 + 16P\bar{x}_2^2) \ , \quad a_5 = \pi^4 k^4 \bar{x}_1^2 \bar{x}_2^2 \ , \quad P = \frac{\pi^4 k}{C_A}\bar{x}_1^2 + C_d k \lambda_1 \ ,$$

$$Q = \frac{16\pi^4 k}{C_A}\bar{x}_2^2 + C_d k \delta_1 \ .$$

In Eq.(14), its general eigenanalysis is quite difficult. However, when $R_a \to 0$, for example, $R_a = 0.0001$, the approximate analysis of the stability of the stationary solutions for system (14) is possible. Neglecting the small terms for R_a in (14), it reduces to

$$\omega^6 + a_1\omega^4 + a_3\omega^2 = 0 \ . \tag{15}$$

From (15), one obtains

$$\omega_{1,2} = 0 \ , \tag{16}$$

and the other four roots satisfy

$$\omega^4 + a_1\omega^2 + a_3 = 0 \ . \tag{17}$$

For the equilibrium point $P_0 = (0, 0, 0, 0, 0, 0)$, it is shown that when $4\lambda_1 + \delta_1 < 0$, this equilibrium point is unstable. While for the equilibrium solution $P_{1,2}$, when $a_1^2 - 4a_3 < 0$, then $\omega^2 = \dfrac{-a_1 \pm i\sqrt{4a_3 - a_1^2}}{2}$. In this case, $\mathrm{Re}(\omega) > 0$ and $\mathrm{Im}(\omega) \neq 0$ may exist. Thus, the two eigenvalues of Eq.(17) may cross the imaginary axis as a conjugate pair. Thus, when the intensity of the convective heating η_0 increases, a Hopf bifurcation to the finite-amplitude periodic solution is possible at the bifurcation point $a_1^2 - 4a_3 = 0$ (Marsden and McCracken, 1976; Shirer and Dutton, 1979; Jin and Ghil, 1990). Setting $\mathrm{Re}(\omega) = 0$, we can obtain the Hopf bifurcation point for η_{0c}. In addition, we note that in Eq.(14), if the convective heating vanishes, then $Re(\omega) < 0$ and $\mathrm{Im}(\omega) \neq 0$. In this case, the stable periodic solutions of system (7) are only found. Thus, the analytical study here shows that both convective heating and nonlinear coupling between vertical modes are responsible for the existence of the Hopf bifurcation. In system (7), when the heating parameter reaches a certain extent, the Hopf bifurcation can occur for the symmetric heating profile and leads to the 30–60-day oscillation. However, for the asymmetric heating profile, can the Hopf bifurcation excite the 30–60-day low-frequency oscillation at the equator? This problem will be investigated numerically in the next subsection.

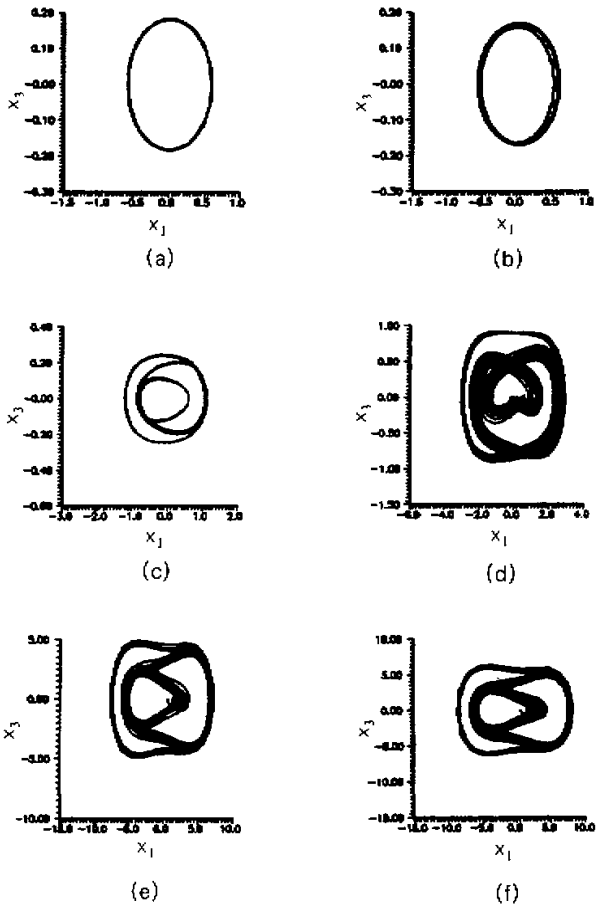

Fig. 5. The phase trajectories in the (x_1, x_3)-plane for the solutions of system (7) for (a) $\eta_0 = 0.0$, (b) $\eta_0 = 0.11$, (c) $\eta_0 = 0.85$, (d) $\eta_0 = 1.5$, (e) $\eta_0 = 5.7$ and (f) $\eta_0 = 7.1$.

5.2 *Numerical results*

5.2.1 *Deep convective heating* ($\delta = -2$)

Here, for $\delta = -2$, if $n_0 = 1$ and the initial data are chosen to be the same as in Fig. 3, then for the zonal wavenumber-one the evolutions of $x_1(t)$ and the phase trajectories in the (x_1, x_3)-plane for the solutions of system (7) for $\eta_0 = 0.0, 0.11, 0.85, 1.5, 5.7$ and 7.1 are shown in Figs. 5 and 6, respectively.

For a given deep convection heating (the maximum heating is located in the upper layer of the troposphere), when the heating parameter η_0 increases, the period-doubling sequences are easily observed. For $\eta_0 = 0.0$, its periodic orbit is the same as in Fig. 3a. While for $\eta_0 = 0.11$, Fig. 5b shows the period-2 orbit with periods corresponding to 15 and 30 days, respectively. When $\eta_0 = 0.85$, a period-3 orbit is found in Fig. 5c. However, when the heating

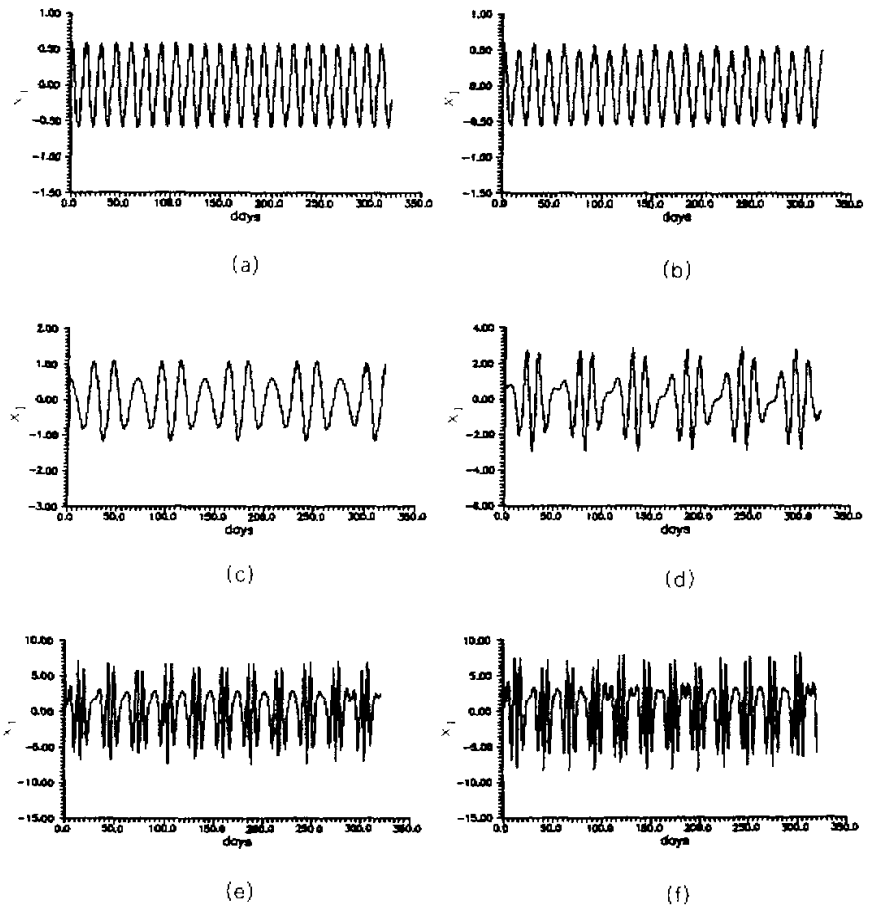

Fig. 6. The time evolution of $x_1(t)$ corresponding to Figs. 5a–5f: (a) $\eta_0 = 0.0$, (b) $\eta_0 = 0.11$, (c) $\eta_0 = 0.85$, (d) $\eta_0 = 1.5$, (e) $\eta_0 = 5.7$ and (f) $\eta_0 = 7.1$.

parameter η_0 further increases, the period-doubling cascade can lead to chaotic solutions as in Figs. 5d–5f. It is clear from Figs. 6d–6f that when $\eta_0 = 1.5 - 7.1$, the principal periods of these chaotic solutions correspond to 56–27 days. Thus, in the equatorial region, the 30–60-day low-frequency oscillation can be excited through the convection heating-related Hopf bifurcation. For zonal wavenumber-two, the 30–60-day oscillation can be excited through this kind of bifurcation only in a narrower parameter domain (figures omitted). While for zonal wavenumber-three, no 30–60-day oscillation can be found. Zhao and Ghil (1991) noted that in an equatorial nonlinear symmetric instability model, only 24–28-day oscillation can be produced through the pitchfork, saddle-node and Hopf bifurcations. Unfortunately, their model cannot explain the 30–60-day oscillation at the equator and its "wavenumber-one" structure. In a numerical model, for a similar deep convection heating profile Lau and Peng (1987) found that the eastward propagation of the low-frequency oscillation arises as a result of the interaction between convection and dynamics by the

so-called mobile wave-CISK mechanism. But, the phase speed of the propagation is much faster than the observed, and depends on the shape of the vertical heating profile. In addition, their numerical experiment result can explain the "wavenumber-1" structure of the low-frequency oscillation. Thus, the comparison between the numerical result of Lau and Peng (1987) and the theoretical result obtained here indicates that our theoretical model is basically appropriate for the 30-60-day oscillation at the equator.

5.2.2 *Shallow convection heating* ($\delta = 2$)

Here, for a shallow convection heating, its numerical calculation is made. It is found that for zonal wavenumber-one, the 30-60-day oscillation can be excited through the Hopf bifurcation, while it is difficult to observe the 30-60-day oscillation for zonal wavenumber-two or wavenumber larger than 2 (figures omitted).

In this paper, our numerical results indicate that for the prescribed three convection heating profiles, the convection heating-related Hopf bifurcation can lead to the 30-60-day oscillation, which does not depend strongly on the vertical distribution of the convection heating. However, as pointed out by Chao (1987), in a linear Kelvin wave-CISK model, the propagation speed of the low-frequency oscillation is related to the vertical heating profile, and the unstable growth for the large wavenumber cannot be inhibited. Crum and Dunkerton (1992) noted that although the "positive-only" nonlinear (conditional) heating was considered in a linear Kelvin wave-CISK model, the scale-selection problem is only modified, but not eliminated. Recently, Cho et al. (1994) pointed out that the scale-selection problem in a linear Kelvin wave-CISK model seems to be eliminated by introducing a phase lag between the maximum cloud heating and the maximum convergence of the Kelvin wave. More recently, Luo (1996) found that in an advective advective nonlinear Kelvin wave-CISK model, the scale-selection problem can also be avoided even if the phase lag between the maximum cloud heating and the maximum convergence of the Kelvin wave was excluded. Unfortunately, he did not discuss the physical mechanism of the occurrence of the 30-60-day oscillation. Here, the 30-60-day oscillation at the equator is found to occur through the convection heating-related Hopf bifurcation.

6. The zonal wind field of nonlinear wavenumber-one Kelvin wave-CISK for sysmmetric heating profile

In this section, in order to further examine whether our model is appropriate for the 30-60-day oscillation at the equator, as an example we will give the vertical structure of the zonal wind of the nonlinear wavenumber-one Kelvin wave-CISK mode for the symmetric heating profile ($\delta = 0.0$). For the same initial data as in Fig. 3, the time-sequence of the zonal wind of the nonlinear wavenumber-one Kelvin wave-CISK mode is shown in Fig. 7 for $\eta_0 = 4.0$.

Fig. 7 shows the vertical structure of the zonal wind field at the semi-wavelength domain. It is found that at day 0, the zonal wind field exhibits a phase reversal between the upper and lower troposphere, and has the easterly and westerly winds in the upper and lower layers of the troposphere, respectively. At day 15, the westerly wind prevails in the upper layer of the troposphere, while the easterly wind prevails in the lower layer. However, the almost same structure as in Fig. 7a reappears at day 30. Thus, in this case, the cycle period of the zonal wind field is nearly 30 days and in agreement with the oscillation period of $x_1(t)$ in Fig. 3c. This indicates that our model seems to be capable of describing the vertical structure of

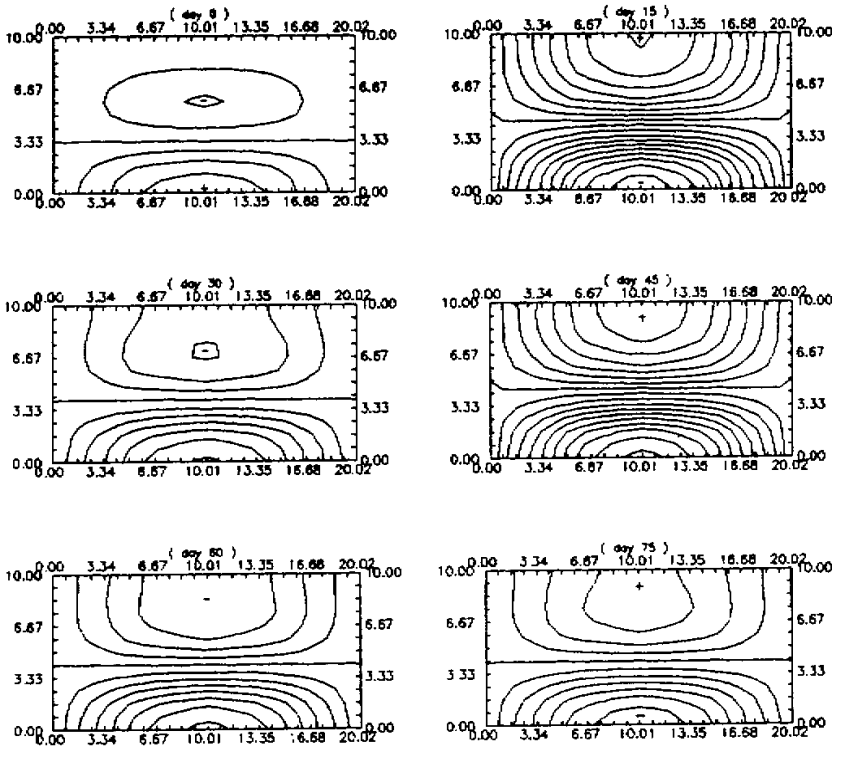

Fig. 7. The time sequences of the zonal wind of nonlinear wavenumber-one Kelvin wave-CISK mode for symmetric heating profile for $\eta_0 = 4.0$, in which the vertical coordinate has been enlarged 10 times. (a) day 0, (b) day 15, (c) day 30, (d) day 45, (e) day 60, (f) day 75. The contour interval is 1.0.

the 30–60-day oscillation at the equator. In addition, the zonal wind field obtained in Fig. 7 is found to be consistent with the numerical experiments done by Lau and Peng (1987) and Hayashi and Golder (1993) (their Fig. 13a) and the observational studies obtained by Hendon and Liebmann (1990) (their Fig. 5a). For zonal wavenumber-two, there is also similar result (figures omitted).

7. Conclusion and discussions

In this paper, we have investigated the bifurcation properties of the nonlinear Kelvin wave-CISK modes with the conditional heating. It is found that for the prescribed three heating profiles, the supercritical pitchfork and Hopf bifurcations are possible when the heating parameter reaches a certain extent. Numerical results show that the convection heating-related Hopf bifurcation can lead to the limit cycle and chaotic solutions. In a wide range of heating parameter, these solutions possess 30–60-day oscillation, and do not depend strongly on the vertical profiles of the convection heating. In addition, the low-frequency solutions are found to possess a phase reversal between the upper and lower troposphere and the

"wavenumber-1" strucutre. Thus, it appears that the convection heating-related Hopf bifurcation might be a possible mechanism of 30-60-day oscillation in the equatorial atmosphere.

It is worthwhile to point out that the other physical mechanisms are excluded in this paper. For example, the phase lag between the maximum cloud heating and the maximum convergence of the Kelvin wave was not considered. In addition, we did not consider the effect of background basic flow and the presence of superclusters (Zhao and Ghil, 1991; Lau et al. 1989; Cho et al., 1994). These problems must be addressed in order to understand the complete dynamical processes leading to the 30-60-day oscillations at the equator.

REFERENCES

Bretherton, C. S., 1988: A theory for nonprecipitating convection between two parallel plates. Part II: Nonlinear theory and cloud field organization. *J. Atmos. Sci.*, **45**, 2391-2415.

Chang, C. P., 1977: Viscous internal gravity waves and low-frequency oscillations in the tropics. *J. Atmos. Sci.*, **34**, 901-910.

Chang, C. P., and H. Lim, 1988: Kelvin wave-CISK: A possible mechanism for the 30-50 day oscillations. *J. Atmos. Sci.*, **45**, 1709-1720.

Chao, W. C., 1987: On the origin of the tropical intraseasonal oscillation. *J. Atmos. Sci.*, **44**, 1940-1949.

Cho, H. R., K. Fraedrich, and J. T. Wang, 1994: Cloud cluster, Kelvin wave-CISK, and the Madden-Julian oscillations in the equatorial troposphere. *J. Atmos. Sci.*, **51**, 68-76.

Crum, F. X., and T. J. Dunkerton, 1992: Analytic and numerical models of wave-CISK with conditional heating. *J. Atmos. Sci.*, **49**, 1693-1708.

Dunkerton, T. J., and F. X. Crum, 1991: Scale selection and propagation of wave-CISK with conditional heating. *J. Meteor. Soc. Japan*, **69**, 702-720.

Feigenbaum, M., 1978: Quantitative universality for a class of nonlinear transformations. *J. Stat. Phys.*, **19**, 25-52.

Ghil, M., and K. C. Mo, 1991: Intraseasonal oscillation in the global atmosphere. Part I: Northern Hemisphere and tropics. *J. Atmos. Sci.*, **48**, 752-790.

Guckenheimer, J., and P. Holmes, 1983: *Nonlinear Oscillations, Dynamical Systems, and Bifurcations of Vector Fields*. Springer-Verlag, 453 pp.

Hayashi, Y., and D. G. Golder, 1993: Tropical 40-50- and 25-30-day oscillations appearing realistic and idealized GFDL climate models and the ECMWF dataset. *J. Atmos. Sci.*, **50**, 464-494.

Hayashi, Y. and D. G. Golder, 1988: Tropical intraseasonal oscillations appearing in a GFDL general circulation model and FGGE data. Part II: Structure. *J. Atmos. Sci.*, **45**, 3017-3033.

Hendon, H. H., and B. Liebmann, 1990: The intraseasonal (30-50 day) oscillation of the Australian summer monsoon. *J. Atmos. Sci.*, **47**, 2909-2923.

Jin, F. F., and M. Ghil, 1990: Intraseasonal oscillations in the extratropics, Hopf bifurcation and topographic instabilities. *J. Atmos. Sci.*, **47**, 3007-3022.

Lau, K. M., and P. H. Chan, 1985: Aspects of the 40-50 day oscillation during the northern winter as inferred from outgoing longwave radiation. *Mon. Wea. Rev.*, **113**, 1889-1909.

Lau, K. M., and P. H. Chan, 1986: Aspects of the 40-50 day oscillation during the northern summer as inferred from outgoing longwave radiation. *Mon. Wea. Rev.*, **114**, 1354-1367.

Lau, K. M., and L. Peng, 1987: Origin of low-frequency (intraseasonal) oscillation in the tropical atmosphere. Part I. The basic theory. *J. Atmos. Sci.*, **44**, 950-972.

Lau, K. M., L. Peng, C. H. Sui and T. Nakazawa, 1989: Dynamics of super cloud cluster, westerly wind bursts, 30-60 day oscillations and ENSO, A unified view. *J. Meteor. Soc. Japan*, **67**, 205-219.

Lim, H., T. K. Lim, and C. P. Chang, 1990: Reexamination of wave-CISK theory: Existence and properties of nonlinear wave-CISK modes. *J. Atmos. Sci.*, **47**, 3078-3091.

Lin, R. Q., F. Busse, and M. Ghil, 1989: Transition to two-dimensional turbulent convection in a rapidly-rotating

annulus. *Geophys. Astrophys. Fluid Dyn.*, **45**, 131–157.

Lorenz, E. N., 1963: Deterministic nonperiodic flow. *J. Atmos. Sci.*, **20**, 130–141.

Luo, D. H., 1996: A simple nonlinear model of low-frequency (intraseasonal) oscillations in the tropical atmosphere. *Nonlinear Processes in Geophysics*, **3**, 29–40.

Madden, R. A., and P. R. Julian, 1971: Detection of a 40–50 day oscillation in the zonal wind in the tropical Pacific. *J. Atmos. Sci.*, **28**, 702–708.

Madden, R. A., and P. R. Julian, 1972: Description of global-scale circulation cells in the tropics with a 40–50 day period. *J. Atmos. Sci.*, **29**, 1109–1123.

Marsden, J. E., and M. McCracken, 1976: The Hopf bifurcation and its applications. *Applied Mathematical Sciences*, **19**, Springer-Verlag, 408 pp.

Miyahara, S., 1987: A simple model of the tropical intraseasonal oscillation. *J. Meteor. Soc. Japan*, **65**, 341–351.

Shirer, H. N., and J. A. Dutton, 1979: The branching hierarchy of multiple solutions in a model of moist convection. *J. Atmos. Sci.*, **36**, 1705–1721.

Sui, C. H., and Lau, K. M., 1989: Origin of low-frequency (intraseasonal) oscillation in the tropical atmosphere. Part III: Low boundary forcings. *J. Atmos. Sci.*, **45**, 37–56.

Takahashi, M., 1987: A theory of the slow phase speed of the intraseasonal oscillation using the wave-CISK. *J. Meteor. Soc. Japan.*, **65**, 42–49.

Van Tuyl, A. H., 1987: Nonlinearities in low-frequency oscillations in the tropics, *J. Atmos. Sci.*, **44**, 2478–2492.

Wang, B., 1988: Dynamics of the tropical low-frequency waves. An analysis of the moist Kelvin waves. *J. Atmos. Sci.*, **45**, 2051–2065.

Wang, B., and Y. Xue, 1992: Behavior of a moist Kelvin wave packet with nonlinear heating. *J. Atmos. Sci.*, **49**, 549–559.

Yost. D. A. and H. N., Shirer, 1982: Bifurcation and stability of low-order steady flows in horizontally and vertically forced convection. *J. Atmos. Sci.*, **39**, 114–125.

Zhao, J. X., and M. Ghil, 1991: Nonlinear symmetric instability and intraseasonal oscillations in the tropical atmosphere. *J. Atmos. Sci.*, **48**, 2552–2568.

Zhao, Y. P. and B. C. Weare, 1994: The effect of diurnal variation of cumulus convection on large-scale low-frequency oscillations in the tropics. *J. Atmos. Sci.*, **51**, 2653–2663.